Structural relaxation and viscosity of Al_2O_3 doped magnesium phosphate glasses

Mária Chromčíková[a,b]*, Branislav Hruška[b], Aleksandra Nowicka[b], Roman Svoboda[c], and Marek Liška[a,b]

[a] *VILA – Joined Glass Centre of the IIC SAS, TnUAD, FChPT STU, Študentská 2, Trenčín, SK-911 50, Slovakia*
[b] *FunGlass, Alexander Dubček University of Trenčín, Študentská 2, Trenčín, SK-911 50, Slovakia*
[c] *University of Pardubice, Faculty of Chemical Technology, Department of Physical Chemistry, Studentská 573, 532 10 Pardubice, Czech Republic*

Abstract

Thermomechanical analysis and differential scanning calorimetry were used to study the viscosity and relaxation behavior of the Al_2O_3-doped magnesium phosphate glasses. Viscosity in the range (10^7 - 10^{11}) Pa·s was described by the nowadays top performing multiparametric models. A fixed extrapolation of high-temperature viscosity according to the Eyring theory was applied with the exception of the Arrhenius equation. The activation energies of viscous flow were very close to the activation energy of enthalpy relaxation determined in terms of the Tool-Narayanaswamy-Moynihan model. On the contrary, the activation energy of volume relaxation was found to be much lower in comparison with the viscous flow activation energy. In general, the increase of the Al_2O_3 content leads to the increases of the viscosity, of the activation energies of viscous flow and structural relaxation (as well as of the kinetic fragilities calculated from these quantities), and of the temperatures characterizing the glass transition during the viscosity, volume, and enthalpy measurements. The phosphate chains interconnecting effect of the Al^{3+} ions was found to be much stronger than the influence of the MgO modifying oxide. However, the enthalpy changes during the relaxation processes seem to be primarily influenced by the MgO/P_2O_5 ratio. Consistence of the compositional interpretation of the obtained results indicates the benefits of the utilization

of the correlation coefficients for attributing the structural units responsible for the changes of physico-chemical quantities.

Keywords: viscosity; structural relaxation; fragility; TMA; Al_2O_3-MgO-P_2O_5 glasses

1. Introduction

Amorphous magnesium phosphate (AMP) is an important material for various bio-applications, mostly used as a biomaterial for bioresorbable orthopedic implants. In [1] the AMP was studied with respect to the utilization for bone void filling applications. The mineralization of AMP was shown to mimic the hydroxyapatite-type characteristic morphology on the substrate surface, and to promote the proliferation and differentiation of the osteoblast-like cells. Recently, a biodegradable, non-exothermic, self-setting orthopedic cement based on AMP was developed [2] by incorporation of the water soluble biocompatible polymer (polyvinyl alcohol, PVA), which enables a controlled growth of the final phase via the biomimetic process. The cement composition with 15 % of PVA in aqueous medium exhibited clinically relevant setting times, mechanical properties and biodegradability. In another application, the composite film of nanostructured amorphous magnesium phosphate and polylactic acid was spin-coated on the surface of the biodegradable AZ31 magnesium alloy [3], significantly improving corrosion resistance and biomineralization capability. This indicates the great potential of the AMP composites in the protective and bioactive coating applications on biodegradable orthopedic magnesium alloys.

Understanding the structural relaxation processes and viscosity behavior is the key factor for the successful practical application of all glassy materials. These processes not only determine the long-term stability of the materials' mechanical properties, but they are also closely related to the glass-forming tendency and manufacturing procedures. Unfortunately, since these properties can be tedious to measure, literature usually lacks the data needed for

considering the manufacturing/processing side of the novel biomaterials. In the present study, the relaxation and viscosity behaviors of the Al_2O_3-doped magnesium phosphate glasses will be reported, where the Al_2O_3 component was added in order to improve the chemical resistivity and anti-corrosive properties (it is well known that the tetrahedral Al ions cross-link with the neighboring phosphor chains by the formation of $AlPO_4$ species that strengthen the glass network [4, 5]). In addition, the utilization of the correlation coefficients between the composition and various physical quantities will be demonstrated, showing the strengths and also the possible weaknesses of this approach.

2. Experimental

Magnesium phosphate glasses doped with Al_2O_3 were prepared by the common melt-quenching procedure. The glasses were prepared by melting the p.a. ammonium dihydrogen phosphate ($NH_4H_2PO_4$) and magnesium carbonate ($MgCO_3$) in alumina crucibles [6]. Appropriate quantities of these compounds were mixed in an agate mortar and placed into alumina crucible. In the first step, the crucible was heated up to 700 °C in an electrical furnace at slow heating rate to remove the water, ammonia and carbon dioxide (calcination). After the calcination, the reaction mixtures were melted in the temperature range 1100 – 1200 °C, depending on their chemical composition. Composition of the prepared glasses was measured by the X-ray fluorescence elemental analyzer S8 Tiger (Bruker) – the contents of the particular components (Al_2O_3, MgO, P_2O_5) are listed in Table 1. The Raman spectrometer inVia Reflex (Renishaw) with Leica DM2500 microscope was used to determine the structure of the prepared glasses. Amorphous nature of the prepared glasses was confirmed by the Panalytical Empyrean DY1098 X-ray diffractometer (XRD) – see the Supplemental online material for the XRD patterns of the prepared amorphous materials. Mass density was measured by the Archimedes method using distilled water. Note that the homogeneity of the

samples was confirmed based on the XRF and Raman measurements performed at various spots on the samples. In addition, the same was done also by DSC, through checking of the glass transition position (which is quite sensitive to the compositional changes).

The volume relaxation and viscosity measurements were realized by the TMA 402 thermomechanical analyzer (Netzsch) – the prismatic samples were cut from the prepared glass ingots (see the Supplemental online material). The dimensions of the prismatic samples were (5x5x20) mm, with the masses approx. (1.5 – 2.0) g. Constant load of 50 mN was applied to the samples in axial deformation during both, the volume relaxation and the viscosity measurements. The volume relaxation measurements were performed by alternating of the cooling and heating steps through the glass transition region. The applied heating rates q^+ and cooling rates q^- were similar in magnitude (5 °C·min^{-1}). The temperature ranges for the TMA cyclic experiments were (292 – 600) °C. The isothermal viscosity experiments were realized at temperatures corresponding to the viscosities of approx. (10^7- 10^{11}) Pa·s. Note that even for the highest applied heating rates the TMA samples were thermally uniform – the temperature gradients across the sample were under all conditions well below 0.2 °C (as determined based on the numerical simulation of the heat transfer).

The enthalpy relaxation experiments were performed via the differential scanning calorimetry (DSC Q2000; TA Instruments) - samples with masses of approx. 10 mg were measured. The measurements were based on the constant ratio (CR) cycles [7]. The samples were cooled and heated in the (420 – 600) °C range; the heating rates q^+ were similar as the preceding cooling q^- rates.

3. Results

The Raman spectra were recorded in the range of (100 – 1500) cm^{-1}; the data were corrected by the Böse-Einstein population factor [8] (see Eq. 1) after the baseline subtraction:

$$I_{\mathrm{cor}} = I_{\mathrm{exp}} \nu \nu_0^3 \frac{1-\exp\left[-hc\nu/kT\right]}{\left(\nu_0 - \nu\right)^4} \tag{1}$$

where I_{exp} and I_{cor} are the observed and corrected Raman intensities, respectively, ν and ν_0 are the Raman shift ant the wavenumber of the excitation laser, respectively, and *h*, *k*, *c*, and *T* represent Planck's constant, Boltzmann's constant, the speed of light, and thermodynamic temperature, respectively. In addition, all spectra were normalized for the maximum intensity to equal unity (see Fig. 1). The Raman bands can be assigned as follows [9-15]: the broad band at ~ 330 cm^{-1} corresponds to the bending vibrations of phosphate polyhedra; the bands in the (650 – 850) cm^{-1} spectral region correspond to the vibrations of the bridging oxygen atoms in the P-O-P chains, in particular the band at ~ 710 cm^{-1} corresponds to the P-O-P symmetric stretch in Q^2 structural units and the band at 795 cm^{-1} corresponds to the P-O-P asymmetric stretch of the oxygen atom in the Q^2 units; the band at 1036 cm^{-1} corresponds to the symmetric stretching vibration of non-bridging oxygen atoms in Q^1 units terminating the metaphosphate chains; the band at 1210 cm^{-1} corresponds to the symmetric stretching motions of the two non-bridging oxygen atoms in the Q^2 tetrahedra; the band at 1280 cm^{-1} corresponds to the asymmetric stretching motions of the two non-bridging oxygen atoms in the Q^2 tetrahedra. Note that the Q^n notation expresses the concentration of the bridging oxygen atoms per tetrahedron by varying the superscript n.

The compositional evolution of the bands' intensities is in a good agreement with the elemental analysis provided by XRF (see Table 1). The structure of the magnesium phosphate glasses largely depends on the magnesium oxide to phosphorous pentoxide molar ratio $y = n(MgO)/n(P_2O_5)$. At the metaphosphate stoichiometry ($y = 1$), the structure constitutes of chains formed by the Q^2 units (PO_4 tetrahedra where two oxygen atoms are shared/bonded with the neighboring PO_4 tetrahedra). At increasing MgO content (for $y > 1$) the structure consists of Q^2 chains terminated by the Q^1 units; the average chain length shortens as the

MgO/P_2O_5 ratio increases. At the pyrophosphate composition (y = 2) the phosphate dimers, two Q^1 connected by a single oxygen atom, are the dominant structural units. [9] This means that for the present compositions the addition of the Mg^{2+} ions (with coordination number equal to 4 [16]) leads to the formation of more diversified structures – note that MgO is known to be a typical modifier oxide that decreases the degree of crosslinking. As the length of the phosphate chains decreases, the averaged distances between the structural units decrease [17] (with the effect being especially prominent in the polyphosphate region, i.e. for y = 1 – 1.5) and the material's density increases. For the present glasses, this behavior was confirmed by experimental measurements, as evidenced by the density values listed in Table 1. Regarding the structural arrangements associated with the addition of Al_2O_3, the Al atoms cross-link with the adjacent chains of PO_4 tetrahedra, resulting in the formation of the $AlPO_4$ units. [5] This largely increases the interconnectivity of the glass matrix, strengthening the network. In addition, the Al^{3+} ions also react with MgO as: $Al_2O_3+MgO = Mg^{2+} +2AlO_2^-$. Since the addition of both oxides, MgO and Al_2O_3, contributes to the increase of the density, further analysis will have to be used to determine the dominant structural unit in this regard – see Section 4 for the corresponding discussion.

Using the compositional information from Table 1, the Shakhmatkin and Vedishcheva thermodynamic model [18] was calculated for the present glasses – the detailed calculations and assumptions are included in the Supplemental online material. Based on this model, only Q^1 and Q^2 structural units are found in the present glasses. The percent representation of the Q^2 chain-forming terahedra is 87.34 % for glass No. 1, 70.78 % for glass No. 2, and 58.49 % for glass No. 3.

The viscosity values were for the studied Al_2O_3-MgO-P_2O_5 glasses determined by TMA based on the following equation:

$$\eta = \frac{Fl}{3S(\mathrm{d}l/\mathrm{d}t)} \tag{2}$$

where F is the loading force, l is the sample height, S is the cross-section of the sample (perpendicular to the applied force), and dl/dt is the deformation rate. The data are shown in Fig. 2 in dependence on temperature in °C as well as on the reciprocal of the thermodynamic temperature (in K). It is apparent that, as the temperature increases, the viscosity of the glasses with higher MgO and Al_2O_3 content decreases more rapidly compared to the compositions with lower MgO and Al_2O_3 contents. Primarily, this is the consequence of the glass matrix being significantly more interconnected via the Al^{3+} ions, which can be confirmed based on the correlation between the composition and log(η/Pa·s). Whereas the correlation coefficient (see Eq. 3 for the definition of correlation coefficient) between the mol.% of Al_2O_3 and the log(η/Pa·s) values determined at the pre-selected temperatures is r = 0.99961, the correlation coefficient between the MgO/P_2O_5 ratio and the same log(η/Pa·s)-T data is only r = 0.95965. This also indicates that the crosslinking caused by Al_2O_3 has much stronger effect compared to the shortening of the phosphate chains originating from the MgO addition.

$$r = \frac{\sum (x-\bar{x})(y-\bar{y})}{\sqrt{\sum (x-\bar{x})^2 \sum (y-\bar{y})^2}} \tag{3}$$

In order to quantify the viscosity behavior, the data from Fig. 2 were described by the three standard viscosity equations - the Vogel-Fulcher-Tammann [19-21] (VFT; Eq. 4), Avramov-Milchev [22] (AM; Eq. 5) and Mauro-Yue-Ellison-Gupta-Allan [23] (MYEGA; Eq. 6):

$$\log\eta = \log\eta_0 + \frac{B}{T - T_0} \tag{4}$$

$$\log\eta = \log\eta_0 + \frac{B'}{T^{C'}} \tag{5}$$

$$\log\eta = \log\eta_0 + \frac{B''}{T} \cdot \exp\left(\frac{C''}{T}\right) \tag{6}$$

where η_0, B, B', B'', T_0, C' and C'' are the parameters of the respective models. The model parameters will be later used to extrapolate the viscosity behavior outside of the measured temperature range and to correlate the results with the structural arrangements in the studied glasses. Therefore, during the non-linear optimization we have adopted a fixed value of $\eta_0 = 4 \cdot 10^{-5}$ Pa.s (in conformity with the Eyring theorem [24]), so that the physically meaningful picture of the viscous flow could be obtained also beyond the data shown in Fig. 2. This option has also the advantage of producing the robust and reliable fits with respect to the possible scatter in the viscosity data. Note that due to the utilization of the Eyring theorem a broad range of viscosities is being described, thus the utilization of the multiparametric equations is both justified and highly necessary. Application of the three models to the present viscosity data is shown in Fig. 3 together with the corresponding sums of squared residuals (SSR). All three models provide similarly good description of the experimental data, with the MYEGA model being very slightly on the top. The fitting parameters of the applied viscosity models are summarized in Table 2. In addition, the viscosity data from Fig. 2 were also fitted by a simple Arrhenius/Andrade equation – see Eq. 7:

$$\eta = \eta_0 \cdot \exp\left(\frac{E_\eta}{RT}\right) \tag{7}$$

where E_η is the viscous flow activation energy. These fitting parameters are also listed in Table 2. In this case, the η_0 parameter was left free for the optimization, otherwise the fit would be very inaccurate; the linear fit of the $\log(\eta/\mathrm{Pa \cdot s})$-$T^{-1}$ dependence cannot account for the overall curvature of the viscosity-temperature dependences in case of the fragile glasses (this point will be further discussed in Section 4).

Thermomechanical analysis was also used for the measurements of structural relaxation, as depicted in Fig. 4. The left-hand graphs show the TMA data (cyclic temperature

program performed in the glass transition region) fitted by the nowadays most often used structural relaxation model – the Tool-Narayanaswamy-Moynihan (TNM) [25-27] set of equations 8 - 10:

$$T_f(T) = T(t) - \int_0^t \mathrm{d}t' \left(\frac{\mathrm{d}T}{\mathrm{d}t} \right) M\left[\xi(t) - \xi(t')\right] \tag{8}$$

where ξ is defined by:

$$\xi(t) = \int_0^t \frac{\mathrm{d}t'}{\tau(t')} \tag{8a}$$

$$M(\xi) = \exp\left(-\xi^{\beta}\right) \tag{9}$$

$$\log \tau\left(T, T_f\right) = A' + x\frac{\Delta h^*}{RT} + (1-x)\frac{\Delta h^*}{RT_f} \tag{10}$$

where T is thermodynamic temperature, t is time, T_f is the so-called fictive temperature (defined as the temperature of the metastable undercooled liquid with the same structure, at the given moment, as is that of the relaxing glass [25]), M is the standard relaxation function [28, 29], β is the non-exponentiality relaxation parameter, x is the non-linearity parameter, A' is the TNM pre-exponential factor, and Δh^* is the structural relaxation activation energy. In order to accommodate Eqs. 8 - 10 to the effect of simultaneously proceeding viscous flow, the following expression was included in the self-made Fortran non-linear optimization program:

$$\varepsilon = \frac{l_2 - l_1}{l_1} \approx \int_{T_1}^{T_2} \alpha_g dT + \int_{T_{f,1}}^{T_{f,2}} \Delta\alpha dT_f - \left(1 + \int_{T_1}^{T_2} \alpha_g dT + \int_{T_{f,1}}^{T_{f,2}} \Delta\alpha dT_f \right) \int_{t_1}^{t_2} \frac{\sigma}{3\eta\left(T, T_f\right)} dt \tag{11}$$

where α_g and α_m are the thermal expansion coefficients of glass and undercooled liquid/melt, $\Delta\alpha$ is defined as $\Delta\alpha = \alpha_m - \alpha_g$, η is viscosity and σ is the axial stress. Note that the relaxation time in Eq. 9 can be replaced by the expression $\eta(t')/K$, where K is the shear modulus.

As results from Fig. 4, the TNM model very well describes the volume relaxation data. The right-hand side graphs in Fig. 4 then show the evolution of the fictive temperature T_f

(as obtained from the non-linear optimization) plotted versus the temperature program of the corresponding cooling-heating cycle. Note that the T_f data exhibit during heating the characteristic behavior typical for the frozen-in glassy structure that requires increased temperature to "catch-up" with the kinetic pseudo-equilibrium of the undercooled liquid. In addition, the volume relaxation data obtained from the TMA were also fitted by the Tool-Narayanaswamy-Mazurin (TNMa) model [30] (Eq. 12 was used instead of Eq. 10 during the non-linear optimization procedure):

$$\log\eta\left(T,T_f\right)=\left(A+\frac{B}{T-T_0}\right)\frac{T_f}{T}+\log\eta_0\left(1-\frac{T_f}{T}\right) \tag{12}$$

where A, B and T_0 are the coefficients of the VFT viscosity equation and η_0 is the limiting dynamic viscosity (tunable parameter in case of the Mazurin's model). Qualitatively very similar results were obtained for both the TNM and TNMa models. The optimized parameters of both models are listed in Table 3 (graphical representation of the TNMa fits is included in the Supplemental online material). The T_g values determined from the cyclic TMA experiments were approx. 542.6 °C (glass No. 1), 553.5 °C (glass No. 2) and 568.5 °C (glass No. 3).

In addition to the volume relaxation, also the enthalpy relaxation experiments were performed by DSC. These were based on the so-called constant ratio (CR) cycles [31], the example of which is shown in the upper graph in Fig. 5. The CR cyclic measurements can be utilized to evaluate the enthalpy relaxation activation energy Δh^* (see Eq. 10 for the TNM model) by employing the following equation (together with the correction factor described in detail e.g. in [31]):

$$-\frac{\Delta h^*}{R}=\left[\frac{\mathrm{d}\ln\left|q^+\right|}{\mathrm{d}\left(1/T_P\right)}\right]_{q^-/q^+=const} \tag{13}$$

where T_p is the temperature of the relaxation peak (overshoot) maximum, and q^+/q^- is the heating/cooling rate ratio. The linearization expressed by Eq. 13 is for the present Al_2O_3-MgO-P_2O_5 glasses shown in the lower graph in Fig. 5. The enthalpy relaxation activation energies determined according Eq. 13 are listed in Table 3. The T_g values determined from the cyclic DSC experiments were approx. 558.1 °C (glass No. 1), 568.8 °C (glass No. 2) and 577.5 °C (glass No. 3).

4. Discussion

The relation between the relaxation motions and the viscous flow process has been the subject of debate for a long time – see e.g. [32-34]. In general, the activation energies of these phenomena are often considered close or even similar. In the present work, we have tested this hypothesis for the three Al_2O_3-doped magnesium phosphate glasses. The activation energies of viscous flow E_η, volume structural relaxation Δh^*_V and enthalpy structural relaxation Δh^*_H are for the studied glasses shown in Fig. 6; the structural relaxation activation energies are depicted in the temperature ranges corresponding to the measurements present in this study (Δh^*_V is further limited to the region of the actual transition between α_g and α_m) . The E_η values were calculated based on Eq. 14:

$$E_\eta = 2.303 \cdot R \cdot \frac{\mathrm{d}(\log \eta)}{\mathrm{d}(1/T)} \tag{14}$$

Interestingly, the extrapolation of the viscous flow activation energies outside of the experimentally measured range brings very large differences in dependence on the used viscosity equation (VFT, AM, MYEGA). Despite the relatively small differences in curvatures shown in Fig. 3 (the log(η/Pa·s)-T fits), the difference between the VFT and AM estimates of E_η may reach over 200 % just 100 °C below the experimentally measured range. Naturally, these differences are much larger for extrapolations to lower temperatures (as opposed to the high-T extrapolations).

There is also a good agreement between the Δh^*_H and E_η values (particularly those predicted by the VFT model). On the other hand, the Δh^*_V values obtained from the curve-fitting of the TMA relaxation experiments are much lower compared to the E_η evaluated in the respective temperature region. Note that the potential issue cannot be the disagreement between the isothermal and non-isothermal conditions and the associated shift of the temperature ranges. For the two activation energies to agree, the volume relaxation measurements would have to be shifted to higher temperatures by approx. 100 °C, which is an unrealistic and physically not meaningful explanation. Theoretically, there is however no reason for the three activation energies to be similar, since each material property (volume, enthalpy, viscous flow) may manifest itself differently in reaction to the similar (or even the same) structural movements.

In addition, the values of activation energies were used to calculate the kinetic fragilities (following the Angell's concept [35]):

$$m_{visc.} = \left.\frac{\mathrm{d}\log\eta}{\mathrm{d}(T_g/T)}\right|_{T=T_g} \cong \frac{E_\eta / R}{T_{12}\ln(10)} \tag{15}$$

$$m_{h^*} = \left.\frac{d\log\tau}{d(T_g/T)}\right|_{T=T_g} \cong \frac{\Delta h^* / R}{T_g \ln(10)} \tag{16}$$

where the T_g and T_{12} were determined from the measurements depicted in Figs. 3 – 5. The fragility values are for the three Al_2O_3-MgO-P_2O_5 glasses plotted in Fig. 7. Each triplet of *m* values corresponds to the evaluation based on the different activation energy, as indicated on the *x*-axis. In agreement with the findings obtained for the activation energies (Fig. 6), also the fragility values calculated for the viscosity and enthalpy relaxation data are in a good agreement, while the kinetic fragility determined for the volume relaxation data is only of 50 – 60 % magnitude compared to the other depicted values. The average fragility indices *m* calculated from the viscosity values are ≈ 51, 56, and 68 for glasses 1, 2, and 3, respectively.

These values of fragility are considered to be rather on the intermediate-to-fragile side, which corresponds to the chain-like structure of the phosphate glasses (the theoretical limits are 16 and 200 for the strong and fragile materials, respectively).

Lastly, we have considered the compositional trends for the quantities reported in the present study and tried to attribute the structural units/components responsible for the particular physico-chemical processes. Intentionally, for this purpose only three glass compositions were included in the present study to show the possibilities provided by this approach. Similarly as previously for the viscosity, we have calculated the correlation coefficients (see Eq. 3) between the compositional dependences of the selected physical quantities and the content of the non-phosphate oxides - expressed as mol.% for Al_2O_3, and as the $n(MgO)/n(P_2O_5)$ ratio for the magnesium oxide. Note that the different expressions were for the two oxides selected purely based on the custom practice with respect to their overall content. The results and conclusions would be similar also for the unified content calculation of any choice. In Table 4 the correlation coefficients are listed for the density ρ, fragility values calculated from different sources (see Fig.7), activation energies of volume Δh^*_V and enthalpy structural relaxation Δh^*_H, T_g values determined by DSC and TMA, and T_{12} values predicted by the three viscosity models (T_{12} VFT, T_{12} AM, T_{12} MYE). The viscosity, fragilities and activation energies (of structural relaxation as well as of viscous flow) seem to be dominantly driven by the crosslinking caused by the Al^{3+} ions (i.e. the correlation coefficients for the Al_2O_3 content were much higher than for the MgO content). Only moderately higher Al_2O_3 correlation coefficients were obtained for the density, T_{12} and T_g determined from TMA. This is particularly interesting with regard to density, where the density increase is undoubtedly caused by both main oxides (MgO and Al_2O_3). However, based on the correlation coefficients mentioned in Table 4 (in addition to the raw magnitudes of the density changes), the Al_2O_3 content has larger impact on the final density. Interestingly,

the T_gs obtained from the DSC measurements show much higher correlation with the MgO content (compared to that of Al_2O_3).

One of the possible interpretations of these findings is that the heat release/consumption changes are dominantly manifesting in association with the movements of the smaller structural unites (shorter phosphate chains) and breakage of the shared tetrahedral interconnections. On the other hand, the volume relaxation appears to be dominantly manifested through the larger-scale simultaneous movements of several adjacent phosphate chains, where the crosslinking via the Al atoms plays the primary role. Correspondingly, the Al_2O_3 content would be in such scenario even more crucial for the viscous flow itself as well as for the apparent energy barriers needed for the initiation of the flow and relaxation processes (as is indeed observed in case of our data – see Table 4).

6. Conclusions

The structural relaxation and viscosity behaviors were studied using TMA and DSC for the Al_2O_3-doped magnesium phosphate glasses. Volume relaxation behavior (measured via cyclic TMA experiments performed in the glass transition region) was described by the TNM and TNMa models in combination with the viscous creep equation. Cyclic enthalpy relaxation measurements were evaluated in terms of the TNM model. The viscosity was described by the MYEGA, AM and VFT models in the (10^7 - 10^{11}) Pa·s range. The activation energies (and the corresponding kinetic fragilities) of viscous flow and enthalpy relaxation were found to be similar – the extrapolation from VFT showed a particularly accurate correspondence with Δh^*_H. On the other hand, the volume relaxation activation energies were found to be significantly lower compared to the E_η values.

Based on the correlation between the composition of the phosphate glasses (MgO and Al_2O_3 contents) and the determined physico-chemical properties, we assume that the enthalpy

changes during the relaxation processes are primarily associated with the movements of the short phosphate chains and disruptions of shared PO_4 tetrahedral units (higher correlation with the MgO/P_2O_5 ratio). The viscous flow and volume changes during the structural relaxation (as well as the activation energies of these processes) then seem to be determined by the crosslinking-driven movements of the adjacent phosphate chains (higher correlation with the Al_2O_3 content). Overall, even a small addition of the Al^{3+} ions was found to results in the large degree of crosslinking, which for the phosphate glasses surpasses the macroscopic manifestation of the modification via MgO. Consistence of the compositional interpretation of the obtained results indicates the benefits of the utilization of the correlation coefficients for attributing the structural units responsible for the changes of physico-chemical quantities.

Acknowledgments
This work was supported by The Slovak Grant Agency for Science under grant No. VEGA 2/0091/20, VEGA 1/0064/18, APVV SK-PL-18-0062 and the project Centre for Functional and Surface Functionalized Glass (CEGLASS), ITMS code is 313011R453, operational program Research and innovation, co-funded from European Regional Development Fund.

References

[1] N. Ostrowski, B. Lee, D. Hong, P.N. Enick, A. Roy, P.N. Kumta. Synthesis, osteoblast and osteoklast viability of amorphous and crystalline tri-magnesium phosphate. ACS Biomater. Sci. Eng. 1 (2015) 52-63.
[2] E. Babaie, B. Lin, V.K. Goel, S.B. Bhaduri. Evaluation of amorphous magnesium phosphate (AMP) based non-exothermic cements. Biomed. Mater. 11 (2016) 055010.
[3] Y. Ren, E. Babaie, S.B. Bhaduri. Nanostructured amorphous magnesium phosphate/poly (lactic acid) composite coating for enhanced corrosion resistance and bioactivity of biodegradable AZ31 magnesium alloy. Prog. Org. Coat. 118 (2018) 1-8.
[4] S.V.G.V.A. Prasad, M.S. Reddy, N. Veeraiah. Nickel ion – A structural probe in BaO-Al_2O_3-P_2O_5 glass system by means of dielectric, spectroscopic and magnetic studies. J. Phys. Chem. Sol. 67 (2006) 2478-2488.
[5] J. Urbánek, J. Hamáček, J. Macháček, J. Kutzendorfer, J. Hubálková. Thermomechanical properties of mullitic materials. Processing and Application of Ceramics 11 (2017) 322-328.

[6] B. Hruška, R. Dagupati, M. Chromčíková, A. Nowicka, J. Macháček, M. Liška, F. Munoz: Thermodynamic model and Raman spectra of MgO-P2O5 glasses. J. Therm. Anal. Calorim. JTAC-D-20-00147 (2019).
[7] R. Svoboda. Utilization of "q^+/q^- = const." DSC cycles for enthalpy relaxation studies. Eur. Polym. J. 59 (2014) 180-188.
[8] R. Shuker, R.W. Gammon. Raman-Scattering Selection-Rule Breaking and the Density of States in Amorphous Materials. Phys. Rev. Lett. 25 (1970) 222.
[9] M.A. Karakassides, A. Saranti, I. Koutselas. Preparation and structural study of binary phosphate glasses with high calcium and/or magnesium content. J. Non-Cryst. Sol. 347 (2004) 69-79.
[10] R.K. Brow, Review: The Structure of Simple Phosphate Glasses J. Non-Cryst. Solids 263 & 264 (2000) 1–28.
[11] J. Koo, B.-S. Bae, H.-K. Na. Raman spectroscopy of copper phosphate glasses. J. Non-Cryst. Solids 212 (1997) 173–179.
[12] J.E. Pemberton, L. Latifzadeh, J.P. Fletcher, S.H. Risbud. Raman spectroscopy of calcium phosphate glasses with varying calcium oxide modifier concentrations Chem. Mater. 3 (1991) 195–200.
[13] R.K. Brow, D.R. Tallant, S.T. Myers, C.C. Phifer. The short-range structure of zinc polyphosphate glass. J. Non-Cryst. Solids 191 (1995) 45–55.
[14] T. Gavenda, O. Gedeon, K. Jurek. Structural and volume changes and their correlation in electron irradiated alkali silicate glasses. Nucl. Instrum. Methods Phys. Res. B 397 (2017) 15-26.
[15] Z. Černošek, J. Holubová. The structure and certain properties of $CaO\text{-}In_2O_3\text{-}P_2O_5$ glasses. J. Non-Cryst. Solids 490 (2018) 44-49.
[16] E. Matsubara, Y. Waseda, M. Ashizuka, E. Ishida. Structural study of Binary phosphate glasses with MgO, ZnO and CaO by X-ray diffraction. J. Non-Cryst. Solids 103 (1988) 117-124.
[17] W. Vogel, Glass Chemistry, Springer, Berlin, 1994.
[18] B.A. Shakhmatkin, N.M. Vedishcheva, M.M. Schultz, A.C. Wright. The thermodynamic properties of oxide glasses and glass-forming liquids amd their chemical structure. J. Non-Cryst. Sol. 177 (1994) 249-256.
[19] H. Vogel. Das Temperaturabhaengigkeitsgesetz der Viskositaet von Fluessigkeiten. Physik Z. 22 (1921) 645.
[20] G.A. Fulcher. Analysis of recent measurements of the viscosity of glasses. J. Am. Ceram. Soc. 8 (1925) 339 – 355.
[21] G. Tammann, W. Hesse. Die Abhangigkeit der Viskositat von der Temperatur bei unterkuhlten Flussigkeiten. Z. Anorg. Allgem. Chem. 156 (1926) 245-257.
[22] I. Avramov, A. Milchev. Effect of disorder on diffusion and viscosity in condensed systems. J. Non-Cryst. Solids 104 (1988) 253.
[23] J. C. Mauro, Y. Yue, A. J. Ellison, P. K. Gupta, D. C. Allan. Viscosity of glass-forming liquids. PNAS 106 (2009) 19780-19784 (2009)
[24] H. Eyring. Viscosity, plasticity, and diffusion as examples of absolute reaction rate. J. Chem. Phys. 4 (1936) 283.
[25] A. Q. Tool. Relation between inelastic deformability and thermal expansion of glass in its annealing range. J. Am. Ceram. Soc. 29 (1946) 240.
[26] O. S. Naraynaswamy. A model of structural relaxation in glass. J. Am. Ceram. Soc. 54 (1971) 491.
[27] C. T. Moynihan, A. J. Easteal, M. A. DeBolt, J. Tucker. Dependence of the fictive temperature of glass on cooling rate. J. Am. Ceram. Soc. 59 (1976) 12.

[28] R. Kohlrausch. Theorie des elektrischen Rückstandes in der Leidner Flasche. Ann. Phys. Chem. 91 (1854) 179–213.
[29] G. Williams, D.C. Watts. Non-Symmetrical Dielectric Relaxation Behavior Arising from a Simple Empirical Decay Function. Trans. Faraday Soc. 66 (1970) 80-85.
[30] O.V. Mazurin, J.K. Starcev, R.J. Chodakovskaja. Relaxacionnaja teorija otzhiga stekla i raschet na jej osnove rezhimov otzhiga. Moskva: Moskovskij chimikotechnologicheskij institut; 1986.
[31] R. Svoboda. Novel equation to determine activation energy of enthalpy relaxation. J. Therm. Anal. Calorim. 121 (2015) 895-899.
[32] I. M. Hodge. Adam-Gibbs formulation of nonlinear enthalpy relaxation. J. Non-Cryst. Sol. 131–133 (1991) 435-441.
[33] M. Chromčiková and M. Liška. Simple relaxation model of the reversible part of the StepScan DSC record of glass transition. J. Therm. Anal. Calorim. 84 (2006) 703-708.
[34] J. Málek, R. Svoboda. Kinetic processes in amorphous materials revealed by thermal analysis: Application to glassy selenium. Molecules 24 (2019) 2725.
[35] C.A. Angell. Relaxation in liquids, polymers and plastic crystals – strong fragile patterns and problems. J. Non-Cryst. Sol. 131 (1991) 13-31.

Figure captions

Fig. 1: Raman spectra of the $MgO\text{-}P_2O_5\text{-}Al_2O_3$ glasses.

Fig. 2: Viscosity values for the $MgO\text{-}P_2O_5\text{-}Al_2O_3$ glasses and depicted in dependence on temperature in °C and in dependence on the reciprocal temperature (in K). For each glass, several measurements were done. The error bars are of approximately 1.5 the magnitude of points.

Fig. 3: Viscosity data for the $MgO\text{-}P_2O_5\text{-}Al_2O_3$ glasses (data from Fig. 2) fitted by the MYEGA, AM and VFT viscosity equations. The error bars are lower than the magnitude of points. Sums of squared residuals attributed to the fits are shown.

Fig. 4: Left column: volume relaxation measurements realized via TMA (points) described in terms of the TNM model (solid line).
Right column: course of T and T_f during the volume relaxation experiments corresponding to the left column graphs.

Fig. 5: Typical enthalpy relaxation cyclic measurement realized via DSC (upper graph) and the evaluation of Δh^*_H using Eq. 13 (lower graph).

Fig. 6: Viscous flow activation energies E_η calculated based on the MYEGA, AM and VFT fits, enthalpy relaxation activation energies Δh^*_H and volume relaxation activation energies Δh^*_V. Errors for Δh^*_H are approximately twice the size of the points.

Fig. 7: Values of kinetic fragility m calculated from different activation energies (indicated on the *x*-axis) using Eqs. 15 and 16.

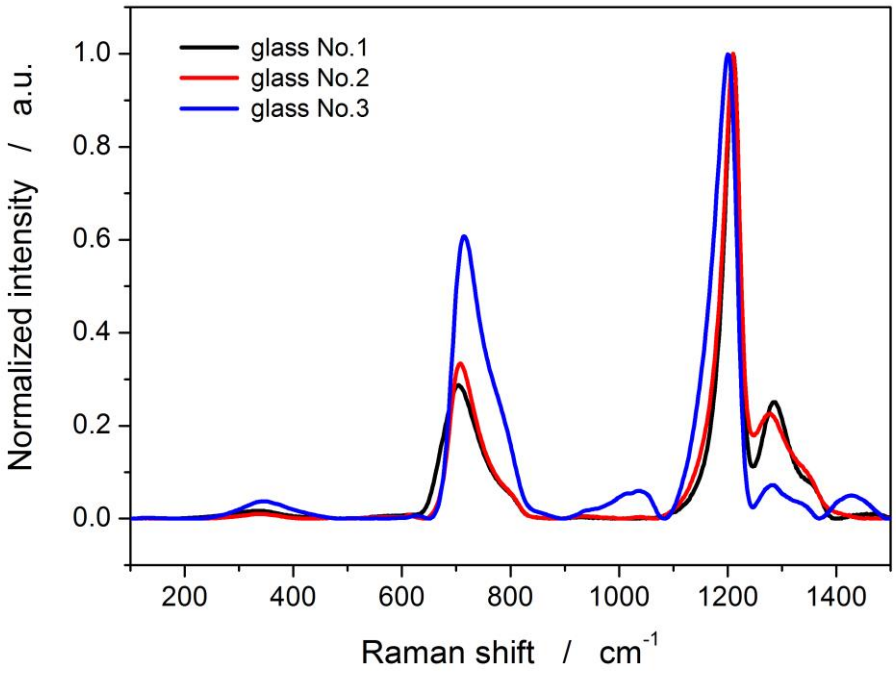

Fig. 1: Raman spectra of the $MgO\text{-}P_2O_5\text{-}Al_2O_3$ glasses.

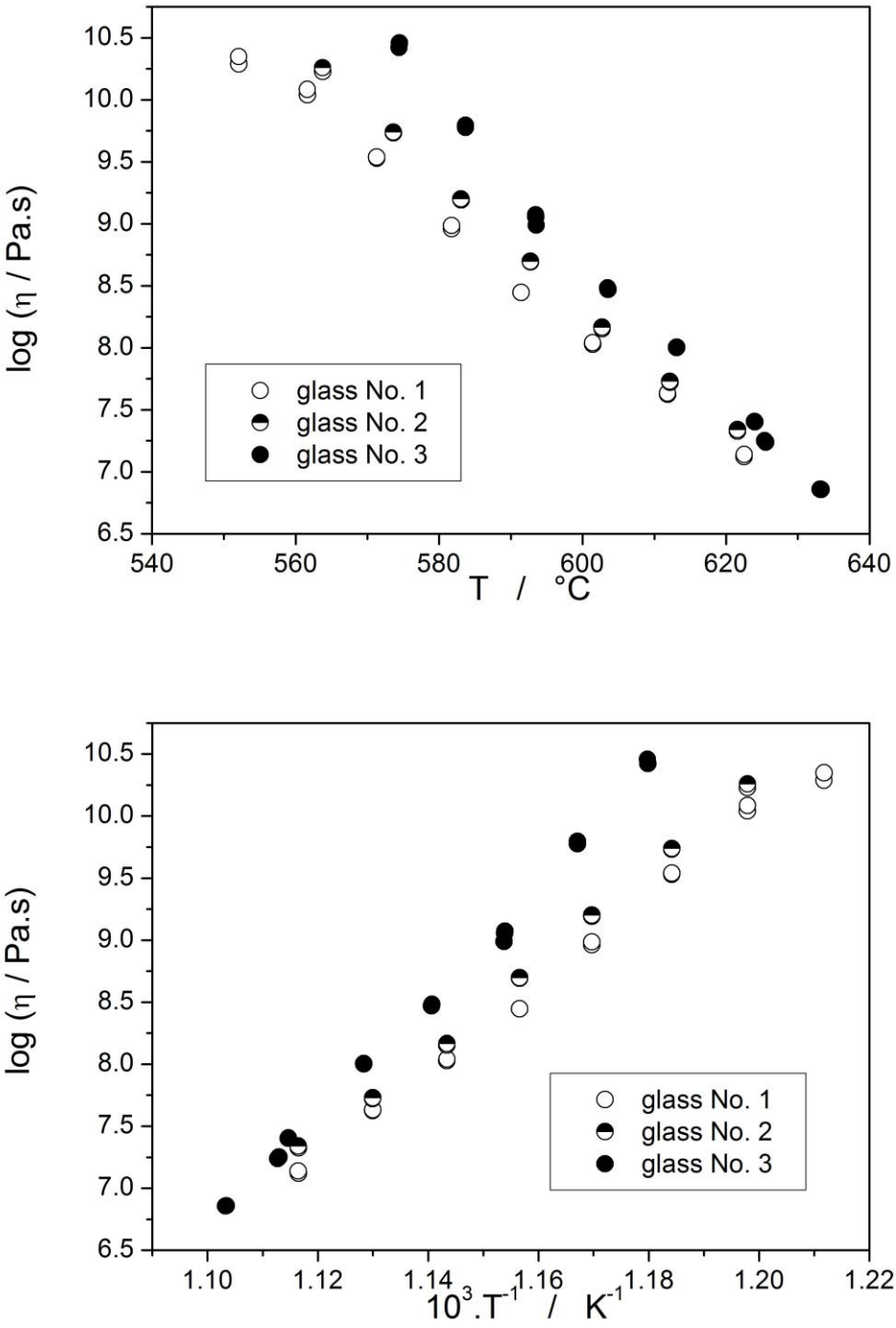

Fig. 2: Viscosity values for the $MgO-P_2O_5-Al_2O_3$ glasses and depicted in dependence on temperature in °C and in dependence on the reciprocal temperature (in K). For each glass, several measurements were done. The error bars are of approximately 1.5 the magnitude of points.

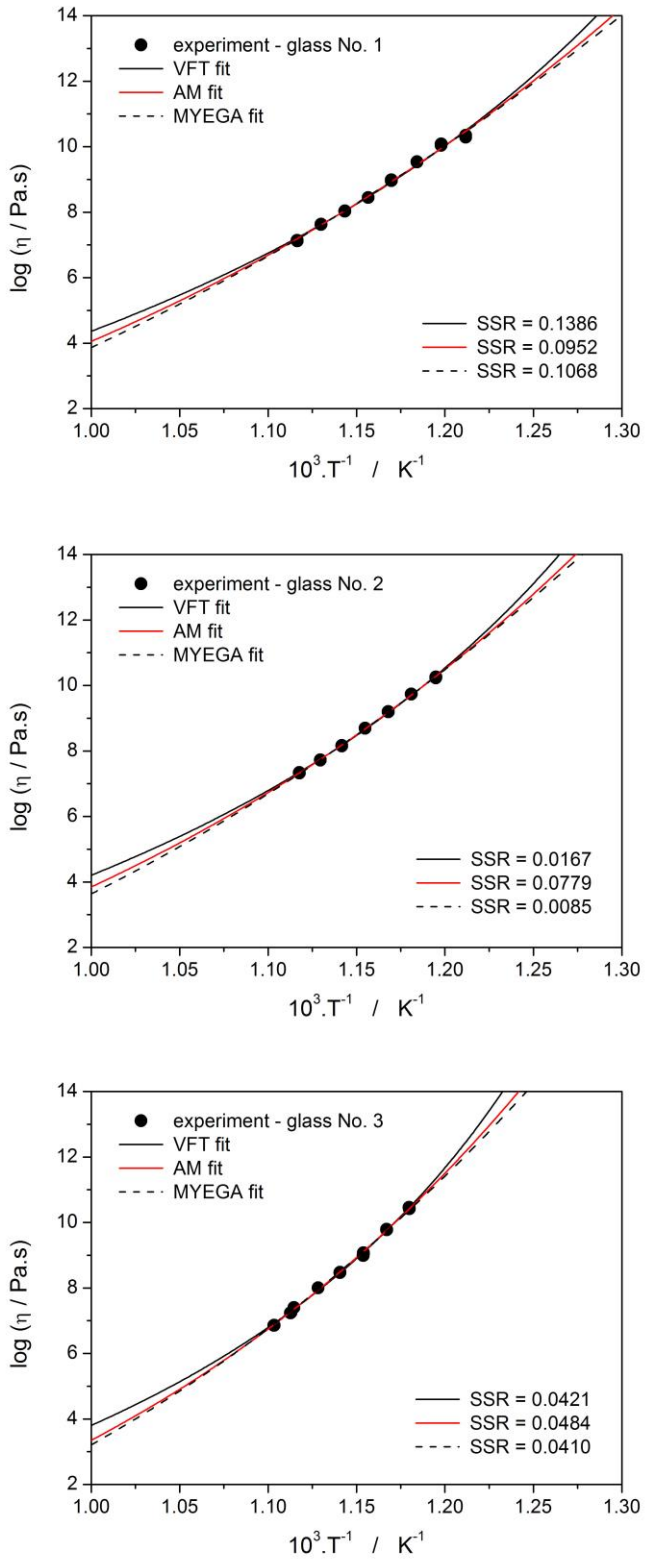

Fig. 3: Viscosity data for the $MgO\text{-}P_2O_5\text{-}Al_2O_3$ glasses (data from Fig. 2) fitted by the MYEGA, AM and VFT viscosity equations. The error bars are lower than the magnitude of points. Sums of squared residuals attributed to the fits are shown.

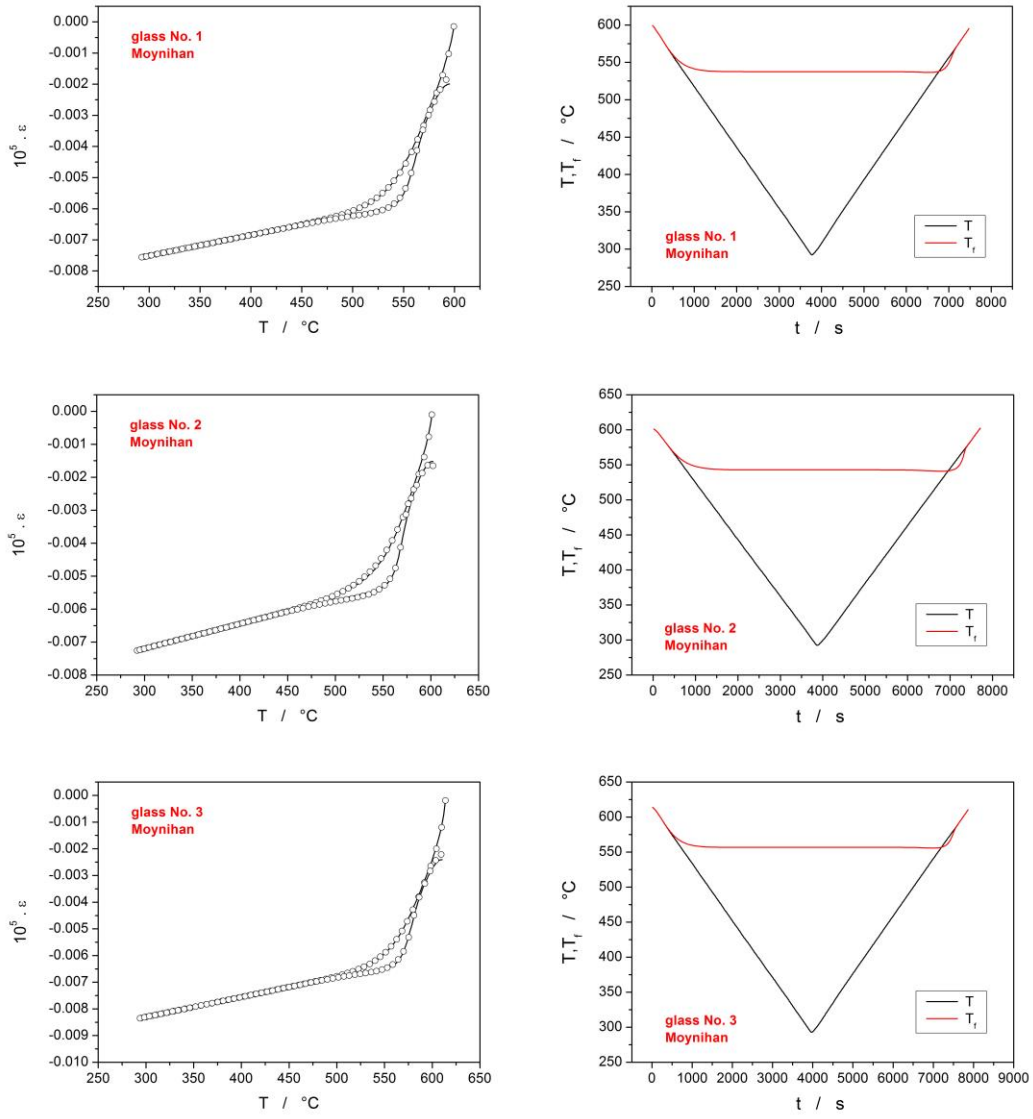

Fig. 4: Left column: volume relaxation measurements realized via TMA (points) described in terms of the TNM model (solid line).
Right column: course of T and T_f during the volume relaxation experiments corresponding to the left column graphs.

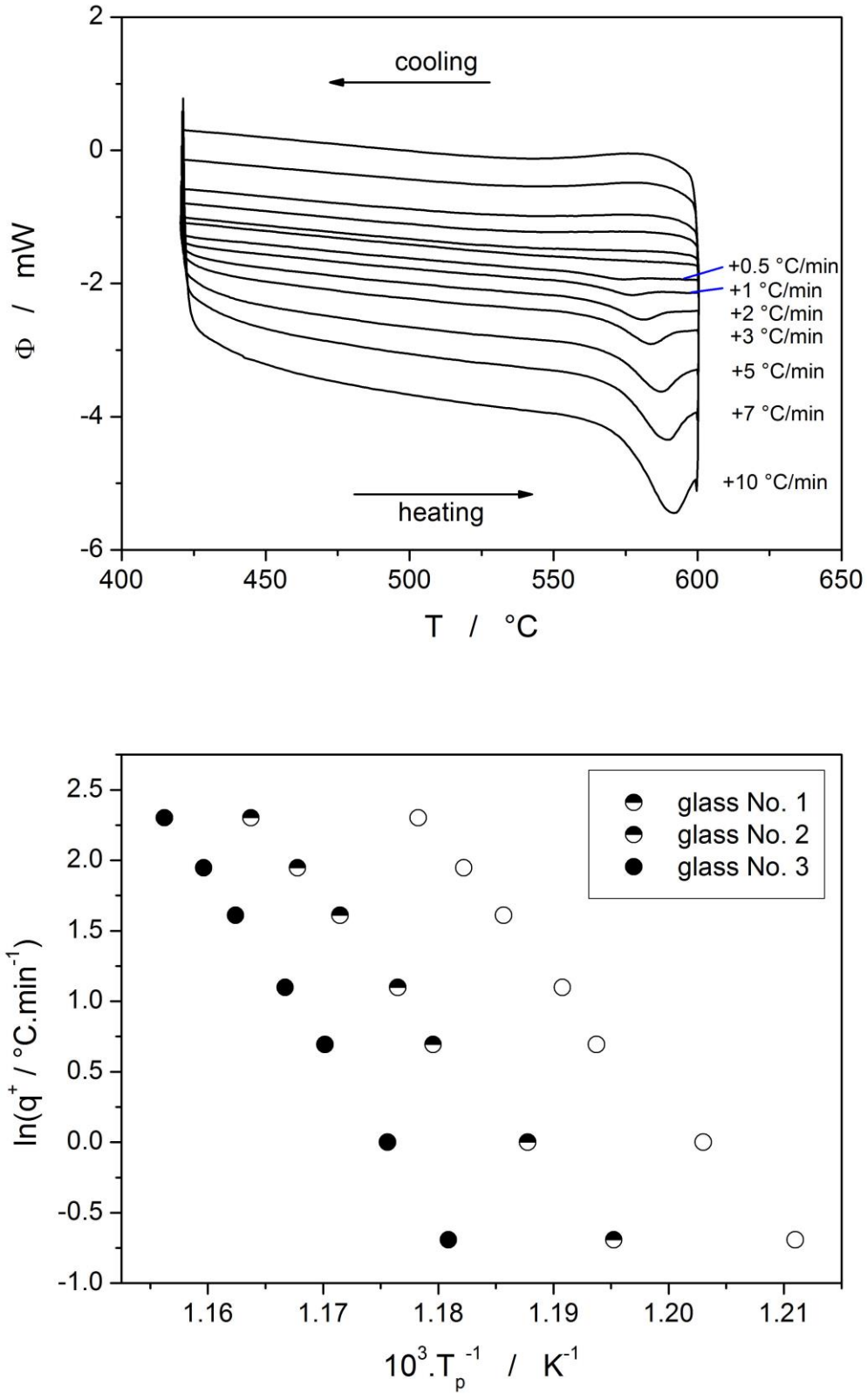

Fig. 5: Typical enthalpy relaxation cyclic measurement realized via DSC (upper graph) and the evaluation of Δh^*_H using Eq. 13 (lower graph).

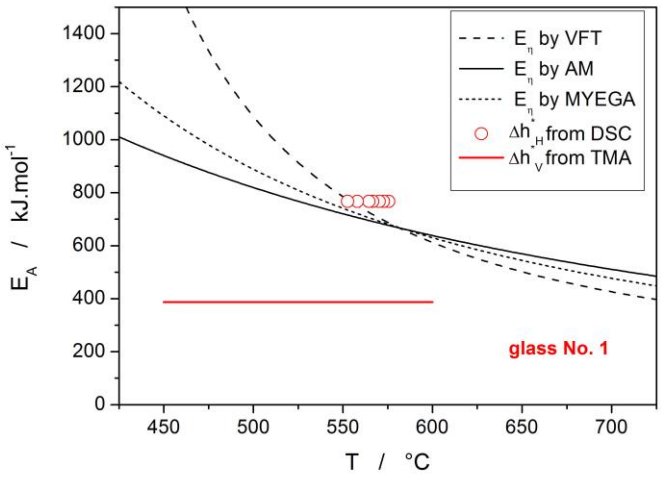

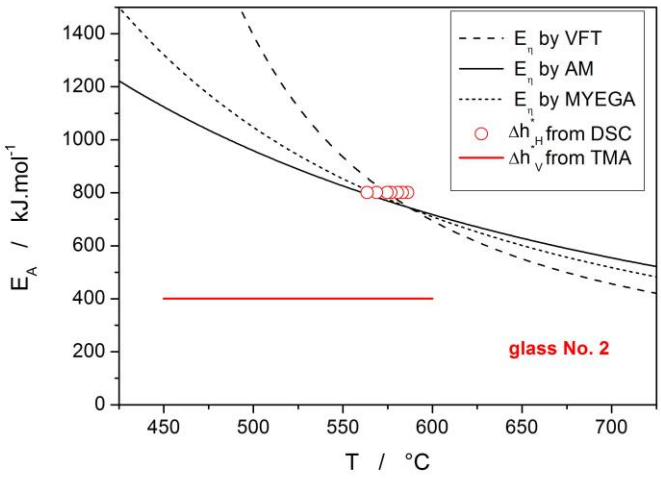

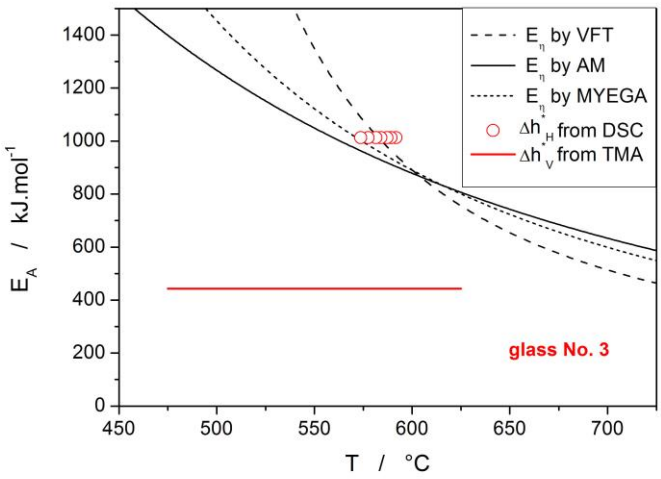

Fig. 6: Viscous flow activation energies E_η calculated based on the MYEGA, AM and VFT fits, enthalpy relaxation activation energies Δh^*_H and volume relaxation activation energies Δh^*_V. Errors for Δh^*_H are approximately twice the size of the points.

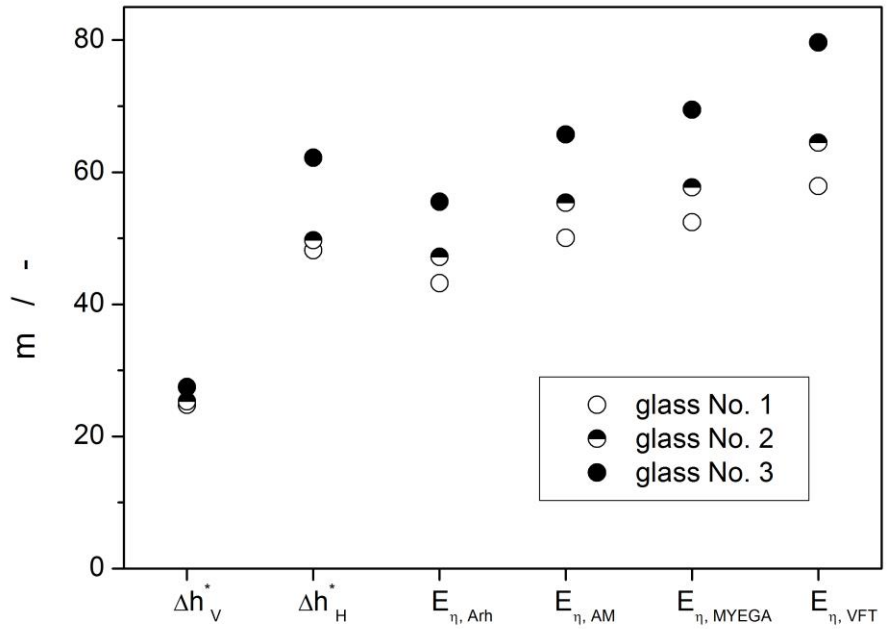

Fig. 7: Values of kinetic fragility m calculated from different activation energies (indicated on the *x*-axis) using Eqs. 15 and 16.

Tables

Table 1: The composition (wt.% and mol.%), abbreviation and densities ρ of the studied glasses as determined by XRF. In addition, also the molar volume of the glasses (corresponding to one mole of P_2O_5) was calculated.

Glass No.	$n(MgO)/n(P_2O_5)$	P_2O_5 wt %	P_2O_5 mol %	MgO wt %	MgO mol %	Al_2O_3 wt %	Al_2O_3 mol %	ρ $g \cdot cm^{-3}$	V_m^{P2O5} $cm^3 \cdot mol^{-1}$
1	1.16	74.05	45.72	24.33	52.90	1.62	1.39	2.415	79.42
2	1.33	71.08	42.16	26.89	56.16	2.03	1.68	2.456	81.33
3	1.48	68.24	39.34	28.65	58.17	3.11	2.50	2.521	82.55

Table 2: VFT, AM and MYEGA parameters obtained for the fits of the $MgO-P_2O_5-Al_2O_3$ viscosities. Parameter $\log\eta_0$ in the equations fixed at $\eta_0 = 4 \cdot 10^{-5}$ Pa.s according [24]. The errors of the fitting parameters were in the order of the last displayed digit.

Glass No.	VFT model			AM model			MYEGA model			Arrhenius	
	$\log\eta_0$	B	T_0	$\log\eta_0$	$\log B'$	C'	$\log\eta_0$	B''	C''	E_η	$\log\eta_0$
1	-4.398	8566	575.5	-4.398	10.442	3.054	-4.398	3346	1761	662	-31.49
2	-4.398	7794	606.7	-4.398	11.407	3.380	-4.398	2457	2045	733	-35.48
3	-4.398	6434	659.5	-4.398	13.279	4.012	-4.398	1222	2681	880	-43.24

Table 3: The values of TNM (Table A) and TNMa (Table B) relaxation models parameters determined for the volume relaxation measurements by non-linear regression analysis.

A) TNM Parameters	**Glass No.1**	**Glass No.2**	**Glass No.3**
$\log\{K/\text{Pa}\}$	9.03 ± 0.02	8.85 ± 0.01	8.97 ± 0.02
β[-]	0.74 ± 0.01	0.84 ± 0.01	0.76 ± 0.01
Δh^*[kJ.mol^{-1}]	387 ± 0.1	400 ± 0.1	443 ± 0.1
x[-]	0.42 ± 0.01	0.31 ± 0.01	0.40 ± 0.01
logA/s	-54.51 ± 0.01	-55.96± 0.01	-61.26± 0.01

B) TNMa Parameters	**Glass No.1**	**Glass No.2**	**Glass No.3**
$\log\{K/\text{Pa}\}$	8.31 ± 0.01	8.30 ± 0.01	8.56 ± 0.01
β[-]	0.77 ± 0.01	0.88 ± 0.01	0.77 ± 0.01
B[K]	34419 ± 1	38063 ± 2	45822 ± 1
E[kJ.mol^{-1}]	286 ± 0.1	316 ± 0.1	381 ± 0.1
$\log\{\eta_0/\text{Pa.s}\}$	-16.62 ± 0.24	-8.00± 0.21	-16.61± 0.20

Table 4: Correlation coefficients between the different thermokinetic quantities and compositional components – mol.% Al_2O_3 content ($n(Al_2O_3)$) and $n(MgO)/n(P_2O_5)$ ratio. The thermokinetic quantities are denoted as follows: density (ρ), fragility calculated from Δh^*_V (m / Δh^*_V), fragility calculated from Δh^*_H (m / Δh^*_H), fragility calculated from Arrhenius E_η (m / E_η AR), fragility calculated from AM E_η (m / E_η AM), fragility calculated from MYEGA E_η (m / E_η M), fragility calculated from VFT E_η (m / E_η V), activation energy of enthalpy relaxation (Δh^*_H), activation energy of volume relaxation (Δh^*_V), T_g from DSC (T_g DSC), T_g from TMA (T_g TMA), T_{12} extrapolated by VFT (T_{12} VFT), T_{12} extrapolated by AM (T_{12} AM), T_{12} extrapolated by MYEGA (T_{12} MYE).

	ρ	m / Δh^*_V	m / Δh^*_H	m / E_η AR	m / E_η AM	m / E_η M	m / E_η V
$n(MgO)/n(P_2O_5)$	0.98502	0.92555	0.88842	0.96771	0.97288	0.96438	0.96219
$n(Al_2O_3)$	0.99028	0.99715	0.98657	0.99831	0.99685	0.99898	0.99932
	Δh^*_H	Δh^*_V	T_g DSC	T_g TMA	T_{12} VFT	T_{12} AM	T_{12} MYE
$n(MgO)/n(P_2O_5)$	0.90186	0.94254	0.99997	0.98960	0.98440	0.98644	0.98405
$n(Al_2O_3)$	0.99105	0.99961	0.94919	0.98583	0.99077	0.98907	0.99103